JOURNAL OF Materials CHEMISTRY

Chemical synthesis of $La_{0.7}Sr_{0.3}MnO_3$/silica homogeneous nanocomposites

Yun-Hui Huang, Chun-Hua Yan,* Sa Wang, Feng Luo, Zhe-Ming Wang, Chun-Sheng Liao and Guang-Xian Xu

State Key Laboratory of Rare Earth Materials Chemistry and Applications, PKU-HKU Joint Laboratory in Rare Earth Materials and Bioinorganic Chemistry, Peking University, Beijing 100871, China. E-mail: chyan@chem.pku.edu.cn

Received 2nd May 2001, Accepted 28th September2001
First published as an Advance Article on the web 25th October 2001

A soft chemistry process to prepare $La_{0.7}Sr_{0.3}MnO_3$ (LSMO)/silica hybrid nanocomposites is reported. Homogeneous granular mixtures are obtained through a sol–gel chemical route by a single step. The precursor solution is comprised of complexes of La^{3+}, Sr^{2+} and Mn^{2+} with ethylenediaminetetraacetic acid (EDTA) and tetraethoxysilane (TEOS). Silica is produced by an ammonia-catalyzed process, and LSMO is obtained by thermal decomposition of the complex precursor. Micrographs from scanning electron microscopy show well homogeneous solid mixtures of the two phases at the nanoscale level. XRD patterns and micro-FTIR analysis indicate that SiO_2 exists in the composites independent of LSMO when calcined at low temperature, whereas Si–O–M (M = La, Sr and Mn) bonds are formed upon calcination above 800 °C. An enhanced magnetoresistance is observed for a 700 °C-calcined (LSMO)$(SiO_2)_{0.20}$ composite from 150 K up to room temperature.

Introduction

Hole-doped manganite perovskites, such as $La_{1-x}Sr_xMnO_3$, have attracted enormous interest for fundamental and practical considerations within the last decade due to the colossal magnetoresistance (CMR) effect .[1–6] Very recently, enhanced low-field magnetoresistance (LFMR) or enhanced room temperature magnetoresistance effects have been successfully achieved for manganite composites with non-magnetic or antiferromagnetic insulating inorganic oxides, which favors potential applications in magnetic switching and recording devices *etc.* Examples can be typically found in ferromagnet/insulator (FM/I) type $La_{2/3}Sr_{1/3}MnO_3/CeO_2$, $La_{0.7}Sr_{0.3}MnO_3/SrTiO_3$ and $La_{0.7}Sr_{0.3}MnO_3$/glass composites, in which the second oxide phase acts as a spin-polarized tunneling barrier for the manganite.[7–10] However, the composites are commonly prepared through a conventional solid state reaction route by mixing the two components mechanically. In comparison, chemical synthesis methods have advantages not only for achieving homogeneous mixing of the components on the atomic scale easily, but also for controlling the microstructures effectively. Thus use of a chemical route is logical for the fabrication of CMR manganite composites.

SiO_2 is a very useful compound in magnetic and magnetoresistive materials. It has been extensively investigated as a non-magnetic matrix in granular films displaying giant magnetoresistance.[11,12] Furthermore, silica can influence the magnetic and conductive properties of some oxide materials. It was reported that the presence of silica could enhance coercivity of Co-ferrite and dielectric constants of metal oxide semiconductors.[13,14] Considering the above-mentioned FM/I type CMR composites, silica is also expected to be an inert insulator that acts as a tunneling barrier for perovskite manganites. Such LSMO/silica composites not only could be promising candidates as CMR materials with improved low-field or room-temperature MR properties, but also relevant examples for further investigating the tunneling mechanism. In addition, the silica surface can be modified with silane coupling agents by direct reaction of the latter with silica gel; surface silanol groups facilitate the introduction of organic groups with covalent binding to the silica surface. Consequently, it is possible to fabricate manganite hybrid composites with special organic and polymer compounds using silica as a covalent linker.

As a traditional synthesis route, silica glass can be obtained by heating alkoxy-derived silica gels. Meanwhile, $La_{0.7}Sr_{0.3}MnO_3$ (LSMO) polycrystallines can be conveniently prepared by thermal decomposition of the precursor complexes, using EDTA as a complexing agent, as described in our previous paper.[15] If the hydrolysis of alkoxides to form silica oxyalkoxy oligomers takes place in the LSMO precursor solution, both silica and LSMO would be formed in the same system, and hence effective combination of the two phases can be achieved *in situ*. Here, we report a sol–gel chemical route to fabricate LSMO/silica nanocomposites, using tetraethoxysilane (TEOS, $Si(OC_2H_5)_4$) as a source of silica. Homogeneous granular mixtures of the two components have been synthesized successfully in a single step. Magnetoresistance effects for these composites were investigated.

Experimental

Stoichiometric amounts (0.7 : 0.3 : 1.0 mol%) of $La(NO_3)_3 \cdot 6H_2O$, $Sr(NO_3)_2$ and $Mn(CH_3CO_2)_2 \cdot 4H_2O$, the starting chemicals for the preparation of $La_{0.7}Sr_{0.3}MnO_3$, were dissolved in an aqueous–ethanol (1 : 1, v/v) mixed solution. Ethylenediaminetetraacetic acid (EDTA) was added as its ammonium salt as a complexing agent to form the La–Sr–Mn–EDTA precursor solution. The molar ratio of total metal ions to EDTA was 1 : 1.5. The silica source, TEOS as an ethanol solution, in calculated molar ratio x was added dropwise to the La–Sr–Mn–EDTA complex solution leading to a transparent uniform precursor solution for the composite. In the resulting solution, the ratio of water and ethanol was 1 : 1 by volume. The solution was adjusted to pH = 9 with aqueous ammonia while stirring. A gel was subsequently obtained due to the hydrolysis of TEOS catalyzed by ammonia. Then the gel was evaporated in a

 DOI: 10.1039/b103922a

porcelain crucible at *ca.* 110 °C to yield a xerogel. The as-prepared xerogel was pre-calcined at 500 °C for 1 h followed by calcination at 600–1000 °C for another 2 h in the furnace under stagnant air to achieve the target composites $(LSMO)(SiO_2)_x$ (x is the molar proportion of silica relative to LSMO).

X-Ray diffraction (XRD) patterns were obtained from a D/max-2000 rotating powder diffractometer (Japan Rigaku) using Cu Kα radiation ($\lambda = 1.5408$ Å) at a scanning rate of $4^\circ\ min^{-1}$ over the 2θ range 20–80°. Thermal decomposition behavior of the uncalcined precursors was studied on a Du Pont 2100 thermal analyzer on 3–4 mg samples in air with a scanning rate of 10 °C min^{-1}. The micro-FTIR spectroscopy measurements were carried out on a Nicolet Magna 750 spectrometer. Cross-sectional morphology was probed by scanning electron microscopy (SEM, 1910FE, AMRAY) under a working voltage of 15.0 kV. The residual C, N and H was analyzed on a Elementar Vario EL (Germany). Resistance was measured on MagLab System 2000 (Oxford, UK) using a standard dc four-probe technique.

Results and discussion

First, calcination behaviors of $(LSMO)(SiO_2)_x$ composites were investigated carefully. Fig. 1 shows combined TGA–DTA runs for xerogels of LSMO and the composite with $x = 0.40$ in air. It is obvious that the two xerogels show a very similar decomposition process. Three weight losses occur in the temperature ranges 210–250, 250–370 and 370–400 °C. The first loss is accompanied by a small endothermic (Endo.) effect at 230 °C, corresponding to the decomposition of residual NH_4NO_3. The second loss is a gradual process without any heat effect, and is attributed to the decomposition of C–H, N–H and some C–C and C–N bonds of EDTA. The final loss is caused by the decomposition of the main C–C and C–N skeletons of EDTA, which is followed by a large exothermic (Exo.) peak centered around 410 °C. This exothermic peak is caused by combustion of organic EDTA.[16] Neither chemical reaction nor other heat variation is found at above 500 °C, indicating that the organic component has been burned out almost completely. The sol–gel process for making silica glass consists of hydrolysis of alkoxides to form silica oxyalkoxy oligomers, which are then condensed to form silica gels. Fig. 2 compares FTIR spectra of TEOS-derived $(LSMO)(SiO_2)_{0.20}$ and pristine LSMO xerogels. The characteristic vibration band of SiO_2 centered at 1100 cm^{-1} (the asymmetric stretching mode of Si–O–Si) and 810 cm^{-1} (the symmetric stretching mode of Si–O–Si) can clearly be observed, as labeled by asterisks in the figure. The TEOS–silica gels are considered to contain mostly SiO_2 and Si–OH groups.[17] In our samples, the stretching vibration band at 3600–3700 cm^{-1} caused by ν(O–H) of Si–OH can not be detected, indicating that TEOS is mostly converted to SiO_2

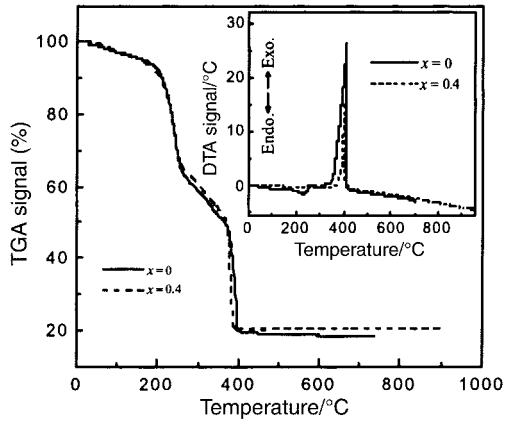

Fig. 1 Combined TGA–DTA runs for the precursor xerogels of $(LSMO)(SiO_2)_x$ with $x = 0$ and 0.40.

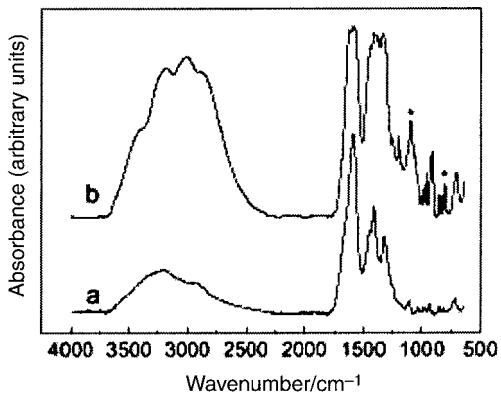

Fig. 2 Micro-FTIR spectra of xerogels for (a) pristine LSMO and (b) TEOS-derived $(LSMO)(SiO_2)_{0.20}$. The peaks labeled by asterisks are caused by Si–O–Si stretching vibrations.

after hydrolysis. The result agrees with the TGA curves which show superposition for the two xerogels. Therefore, the total reaction can be written as below:

$$Si(OC_2H_5)_4 + 4H_2O \rightarrow Si(OH)_4 + 4C_2H_5OH \quad (1)$$

$$nSi(OH)_4 \rightarrow nSiO_2 + 2nH_2O \quad (2)$$

Furthermore, it is necessary to know how silica influences the calcination behavior and crystallization of LSMO. The exothermal effect can be estimated by $\Delta H/gk$, which equates to a given thermal peak area over the taken sample weight in a DTA curve, and is given in the following equation:

$$\Delta H/gk = \frac{\int_{t_1}^{t_2} \Delta T \mathrm{d}t}{m} \quad (3)$$

where, m is the reactant mass, ΔH the reaction enthalpy, g the geometric constant of the used instrument, k the thermal conductivity constant, ΔT the temperature difference, t_1 the integral lower limit, and t_2 the integral upper limit, respectively. The value of $\Delta H/gk$ is 144, 116, 79 and 40 $°C^2\ mg^{-1}$ for $x = 0$, 0.10, 0.20 and 0.40, respectively, showing a decrease with increasing x. The exothermic heat accelerates the successive solid state diffusion reaction and manganite formation. Excessive addition of silica will prevent the combustion of EDTA. However, the external heating provided should be adequate for crystallization of the perovskite in the composites. Table 1 exhibits the impurity weight contents in the composites calcined at 1000 °C for 2 h. The total C, H and N content is less than 0.5 wt% for $x = 0$, and 0.6 wt% or so for the other composites. Thus it can be considered that silica introduction does not affect the purity of the final samples. On the other hand, the observed small change in C and H contents between the pristine LSMO and LSMO/silica composites indicates that the carbon in TEOS has been almost completely burned off during calcination.

Fig. 3(a) shows XRD patterns of $(LSMO)(SiO_2)_x$ with $x = 0.20$ calcined at different temperatures (T_{cal}) for 2 h. It is notable that only the diffraction peaks of LSMO perovskite are observed upon calcination at 600 and 700 °C. Because the silica is non-crystalline, it shows no diffraction peaks as confirmed by our experimental data and the silica and LSMO remain as segregated phases. However, at $T_{cal} = 800$ °C, additional peaks

Table 1 Elemental analysis results of impurities in the $(LSMO)(SiO_2)_x$ composites calcined at 1000 °C for 2 h

Silica content x	0	0.10	0.20	0.40
C (wt%)	0.194	0.206	0.233	0.239
H (wt%)	0.160	0.161	0.211	0.241
N (wt%)	0.095	0.228	0.202	0.154

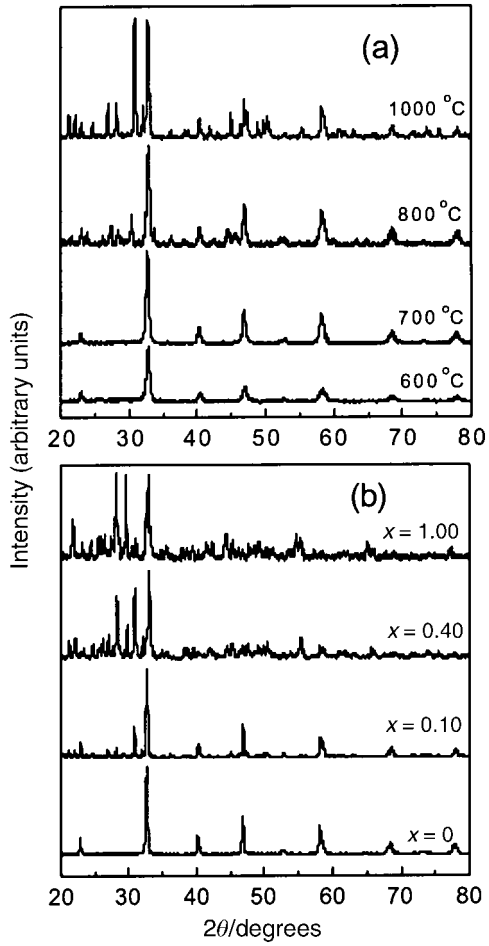

Fig. 3 (a) XRD patterns of $(LSMO)(SiO_2)_x$ with $x=0.20$ calcined at different temperatures for 2 h; (b) XRD patterns of the samples with $x=0$, 0.10, 0.40 and 1.00 calcined at 1000 °C for 2 h.

are observed besides the peaks of LSMO. These are mainly caused by the apatite-type silicate $La_8Z_2(SiO_4)_6O_2$ ($Z=Mn^{2+}$ or Sr^{2+}) (JCPDS No. 38–283). This apatite is a hexagonal structure with a three dimensional network connected by MO_6 (M is mainly La) octahedra and SiO_4 tetrahedra. Fig. 3(b) compares the XRD patterns of $(LSMO)(SiO_2)_x$ with $x=0$, 0.10, 0.40 and 1.00 calcined at 1000 °C for 2 h. The diffraction peaks caused by LSMO are clearly observed in the XRD patterns even for the composite with high silica content. This demonstrates that $La_{0.7}Sr_{0.3}MnO_3$ can be successfully formed in the presence of silica. However, when $x\geqslant 0.40$, it is observable from the patterns that LSMO is poorly crystallized, and some other phases, including $La_8Z_2(SiO_4)_6O_2$ and a possible Si-rich phase, are evident. In the case of high silica content in the composite, the amorphous SiO_2 will block the diffusion of metal ions during the solid state reaction, which is unfavorable for perovskite formation.

Micro-FTIR spectra were measured to further investigate the interaction between the silica and LSMO. As depicted in Fig. 4, for the pure SiO_2, a characteristic absorption of 1100 cm^{-1} corresponds to the asymmetric ν(Si–O–Si) stretching vibration,[18] and the peak at wavenumber of 810 cm^{-1} is due to the symmetric vibration of Si–O–Si.[19] We take the composite of $x=0.20$ as an example. When $T_{cal}=600$–800 °C, the main absorption band is still centered at 1100 cm^{-1} and the peak of 800 cm^{-1} also appears, demonstrating that the silica exists as a segregated amorphous phase in the composite, which reinforces the XRD results. When $T_{cal}=1000$ °C, the ν(Si–O–Si) peak shifts to a lower wavenumber of 950 cm^{-1}. A similar downshift was also found in an Si–O–Ti system.[20] Therefore, we take into account that Si–O–M (M = La, Sr and Mn) bonds

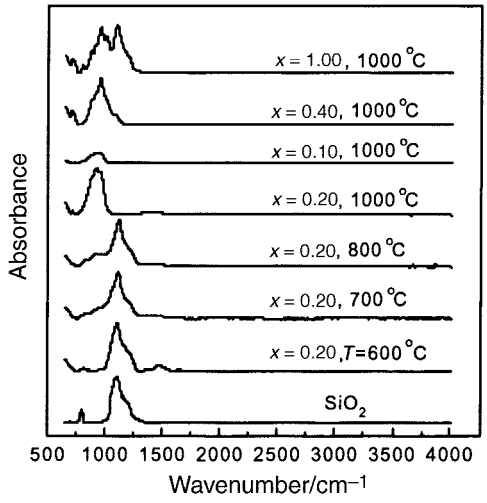

Fig. 4 Micro-FTIR spectra of $(LSMO)(SiO_2)_x$ composites with $x=0.10$, 0.20 and 0.40 calcined at different temperatures.

are formed upon high temperature calcination. This is in agreement with the XRD results. Because of the formation of the oxyapatite $La_8Z_2(SiO_4)_6O_2$ in this case, Si–O–M bonds are present.[21] In addition, Fig. 4 also shows FTIR spectra of 1000 °C-calcined $(LSMO)(SiO_2)_x$ with different values of x. The band for the asymmetric ν(Si–O–M) stretching vibration is observed for $x=0.10$–1.00, and its intensity increases with the silica content. It is clear that bands at 950 and 1100 cm^{-1} appear for $x=1.00$, showing the coexistence of Si–O–M and Si–O–Si bonds. Therefore, we believe that silica and silicate coexist in the $(LSMO)(SiO_2)_{1.00}$ composites calcined at 1000 °C. The attachment points between the silica network and the LSMO surface are probably established through the formation of Si–O–M bonds or other weak interactions at the interfaces.

The variation of silica morphology with calcination temperature can be directly observed by SEM images. Fig. 5(a)–(c)

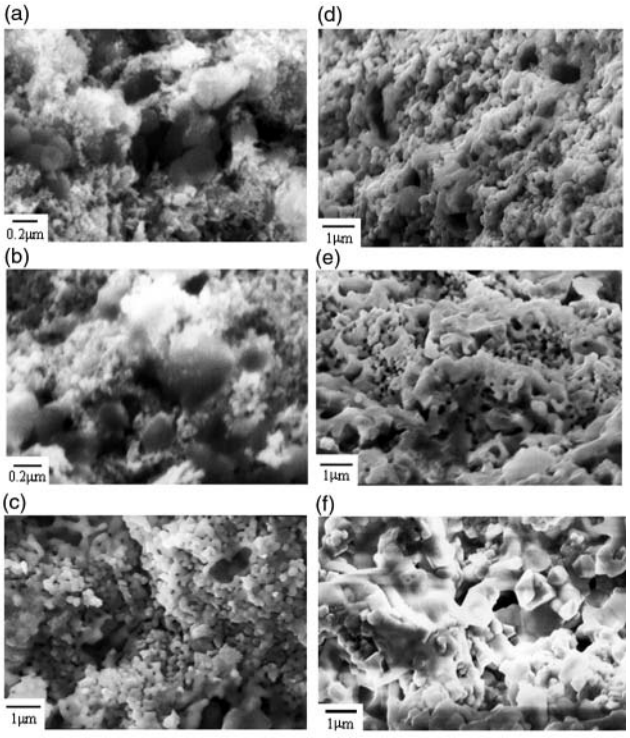

Fig. 5 Cross-sectional SEM micrographs for $(LSMO)(SiO_2)_x$ pellets: (a) $x=0.20$, $T_{cal}=600$ °C; (b) $x=0.20$, $T_{cal}=700$ °C; (c) $x=0.20$, $T_{cal}=1000$ °C; (d) $x=0.10$, $T_{cal}=1000$ °C; (e) $x=0.40$, $T_{cal}=1000$ °C; (f) $x=1.00$, $T_{cal}=1000$ °C.

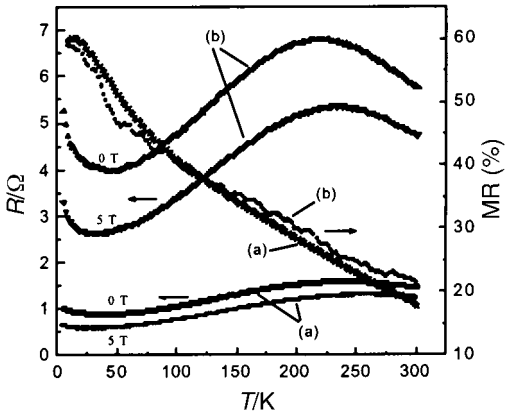

Fig. 6 Temperature dependence of resistance and MR ratio obtained at 5 T for (a) LSMO and (b) $(LSMO)(SiO_2)_{0.20}$ calcined at 700 °C.

shows SEM micrographs of the composite with $x=0.20$ obtained at different T_{cal}. For $T_{cal}=600$ and 700 °C, the observed spherical grains with diameter of about 200 nm are silica particles embedded into the LSMO matrix. When $T_{cal}=1000$ °C, the silica grains are no longer spherical, but connect tightly with LSMO nanoscale grains. A similar appearance is also found in other composites with $x=0.10$, 0.40 and 1.00, as shown in Fig. 5(d)–(f). Two different phases of LSMO and silica can clearly be distinguished from each other. The LSMO grains retain good spherical shapes, which are relatively uniform with estimated sizes within 100–150 nm. For the composites with low SiO_2 content, some LSMO grains connect with each other, and some adhere to the silica surface while for the SiO_2-rich composites, LSMO grains are attached on silica networks. As x increases, the situation of silica embedded in LSMO matrices changes to that of some LSMO grains embedded in silica matrices. Apatite-like silicates are found to occur at the interfaces between LSMO and silica.

Fig. 6 displays the temperature dependence of the resistance and MR ratio (defined as $(R_{0T}-R_{5T})/R_{5T}$) for LSMO and $(LSMO)(SiO_2)_{0.20}$ calcined at 700 °C. It is found that the presence of SiO_2 in LSMO matrices results in an increase of resistance and a lowering of the metal–insulator transition. This can well be explained by enhanced grain boundary effects caused by insulating SiO_2. Interestingly, the MR of the composite is larger when $T>150$ K and lower when $T<150$ K than that of LSMO, which means that MR enhancement occurs in the high temperature range. For example, the MR at 300 K is 21.4% for $(LSMO)(SiO_2)_{0.20}$ and 17.7% for LSMO. Thus the combination between LSMO and SiO_2 may be an effective way to achieve improved MR at room temperature. The influence of SiO_2 with different sizes and phase status on the MR properties and the mechanism of the enhancement will be subsequently published elsewhere in detail.

Conclusions

A soft chemical route, comprising thermal decomposition of metal–EDTA complex precursors and ammonia-catalyzed hydrolysis of TEOS, has successfully been used to prepare $La_{0.7}Sr_{0.3}MnO_3$/silica nanocomposites by a single step. Using this simple synthesis process, well homogeneous solid mixtures can be effectively prepared. Moreover, the microstructure of the composites can be controlled mainly through the calcination temperature. When calcined at above 800 °C, silica undergoes some interaction with LSMO and Si–O–metal bonds are formed, which may establish the connection between the silica network and the LSMO surface.

Acknowledgements

We appreciate the financial support provided by MOST of China (G1998061310, State Key Project of Fundamental Research), NSFC (Nos. 29831010 & 20023005), the Post-Doctoral Foundation of China, and Founder Foundation of PKU.

References

1 R. V. Helmolt, J. Weoker, B. Holzapfel and K. Samwer, *Phys. Rev. Lett.*, 1993, **71**, 2331.
2 S. Jin, T. H. Tiefel, M. Mocormack, R. A. Fastnacht, R. Ramesh and L. H. Chen, *Science*, 1994, **264**, 413.
3 H. Y. Hwang, S. W. Cheong, N. P. Ong and B. Batlogg, *Phys. Rev. Lett.*, 1996, **77**, 2041.
4 A. Gupta, G. Q. Gong, G. Xiao, P. R. Duncombe, L. Pecoeur, P. Trouilloud, Y. Wang, V. P. Dravid and J. Z. Sun, *Phys. Rev. B*, 1996, **54**, 15629.
5 T. Walter, K. Dorr, K.-H. Muller, B. Holzapfel, D. Eckert, M. Wolf, D. Schlafer, L. Schultz and R. Grotzschel, *Appl. Phys. Lett.*, 1999, **74**, 2218.
6 X. L. Wang, S. X. Dou, H. K. Liu, M. Ionescu and B. Zeimetz, *Appl. Phys. Lett.*, 1998, **73**, 396.
7 LI. Balcells, A. E. Carrillo, B. Martinez and J. Fontcuberta, *Appl. Phys. Lett.*, 1999, **74**, 4014.
8 O. A. Shlyakhtin, Y. J. Oh and Y. D. Tretyakov, *Solid State Commun.*, 2001, **117**, 261.
9 J.-M. Liu, Y. G. Luan, H. Sang, Z. C. Wu, X. Y. Chen, Z. G. Liu, Y. W. Du, Q. Huang and C. K. Ong, *Appl. Phys. Lett.*, 2001, **78**, 1110.
10 S. Gupta, R. Ranjit, C. Mitra, P. Raychaudhuri and R. Pinto, *Appl. Phys. Lett.*, 2001, **78**, 362.
11 A. Milner, A. Gerber, B. Groisman, M. Karpovsky and A. Gladkikh, *Phys. Rev. B*, 1996, **76**, 475.
12 S. Sanker, A. E. Berkowitz and D. J. Smith, *Phys. Rev. B*, 2000, **62**, 14273.
13 J. Ding, Y. J. Chen and S. Wang, *Appl. Phys. Lett.*, 2000, **77**, 3621.
14 G. Lucovsky and G. B. Rayner Jr., *Appl. Phys. Lett.*, 2000, **77**, 2912.
15 Y. H. Huang, Z. G. Xu, C. H. Yan, Z. M. Wang, T. Zhu, C. S. Liao, S. Gao and G. X. Xu, *Solid State Commun.*, 2000, **114**, 43.
16 Y. W. Zhang, J. T. Jia, C. S. Liao and C. H. Yan, *J. Mater. Chem.*, 2000, **10**, 2137.
17 K. Kamiya, T. Dohkai, M. Wada, T. Hashimoto, J. Matsuoka and H. Nasu, *J. Non-Cryst. Solids*, 1998, **240**, 202.
18 A. Duran, C. Serna, V. Fornes and J. M. Fernandez-Navarro, *J. Non-Cryst. Solids*, 1986, **82**, 69.
19 M. Schraml-Marth, K. L. Walther, A. Wokaun, B. E. Haudy and A. Baiker, *J. Non-Cryst. Solids*, 1992, **143**, 93.
20 D. C. M. Dutoit, M. Schmeider and A. Baiker, *J. Catal.*, 1995, **153**, 165.
21 J. Felsche, *J. Solid State Chem.*, 1972, **5**, 266.